Unveiling interaction potential surface between drug-entrapped polymeric micelles clarifying the high drug nanocarrier efficiency

Takeshi Morita,[1,] Sayaka Mukaide,[2] Ziqiao Chen,[2] Kenjirou Higashi,[2,]* Hiroshi Imamura,[3] Kunikazu Moribe,[2] and Tomonari Sumi[4,]**

1. Graduate School of Science, Chiba University, Chiba 263-8522, Japan

2. Graduate School of Pharmaceutical Sciences, Chiba University, Chiba 260-8675, Japan

3. College of Life Sciences, Ritsumeikan University, Shiga 525-8577, Japan

4. Research Institute for Interdisciplinary Science, Okayama University, Okayama 700-8530, Japan

ABSTRACT.

Polymeric micelles are invaluable media as drug nanocarriers. Although knowledge of an interaction between the micelles is a key to understanding the mechanisms and developing the superior functions, interaction potential surface between drug-incorporated polymeric micelles has not yet been quantitatively evaluated due to the extremely complex structure. Here, interaction potential surface between drug-entrapped polymeric micelles was unveiled by combining a small-angle scattering experiment and a model-potential-free liquid–state theory. Triblock copolymer composed of poly(ethylene oxide) and poly(propylene oxide) was investigated over wide concentration range (0.5–10.0wt%). Effects of entrapment of water-insoluble hydrophobic drug, cyclosporin A, on the interaction were explored by comparing the interactions with and without the drug. The results directly clarified the high drug carrier efficiency in terms of the interaction between the micelles. In addition, investigation based on density functional theory provided a deeper insight into the monomer contribution to the extremely stable dispersion of the nanocarrier.

KEYWORDS.

polymeric micelle, drug entrapment, nanocarrier, interaction potential surface, small-angle X-ray scattering, model-potential-free liquid–state theory

INTRODUCTION

Polymeric micelles are beneficial media as drug nanocarriers with various functionalities such as delivery efficiency enhancement, stable dispersion under drug incorporation, and specific drug releasability.[1-3] Effects of drug encapsulation and additive compounds on the micelle structure have been intensively studied using various methods such as small-angle scattering[4-9] and dynamic light scattering,[8-11] as well as investigations of the neat micelles.[12] Equally, the knowledge of the interaction between the polymeric micelles is a key to understanding their mechanisms and developing the superior functions. However, the interaction potential surface between the drug-incorporated polymeric micelles has not been quantitatively evaluated due to the extremely complicated micelle structure.

To achieve obtaining the knowledge, we adapted two approaches in this study: (1) Aggregation interaction between the polymeric micelles as well as the repulsive force was considered for evaluation of the spatial structure between the micelles without simplifying the interactions. (2) Transformation of the spatial structure into an interaction potential surface was calculated without eliminating any of the interactions using a model-potential-free (MPF) liquid–state theory. The MPF theory[13-17] enables us to realize potential surface in complex systems without eliminating the interaction forces, as it did not require any specific model-potential functions. The DLVO model is commonly applied to evaluate the potential surface between colloid particles with electrostatic interaction.[18,19] The attractive force is often replaced by a Yukawa-type potential with variable parameters to account for specific interactions induced by investigated systems.[20,21] Unfortunately, using the DLVO-type or Yukawa-type potential model, it is difficult to quantitatively solve potential surface in complex systems because these introduced model-functions cause limited expression for the quantitative profile.

Here, the interaction potential surface between drug-entrapped polymeric micelles was unveiled by combining small-angle X-ray scattering (SAXS) experiments and the MPF theory. Poly(ethylene oxide) (PEO) and poly(propylene oxide) (PPO) triblock copolymer ($EO_{101}PO_{56}EO_{101}$), poloxamer 407 (P407), was investigated as the typical nanocarrier. P407 micelle specifically shows the high stability of the aggregates and the hydrogels.[3] This property leads to important characteristics as a drug carrier, namely the sustained drug releasability. The knowledge of how to interact between micelles each other is, therefore, of particular importance for understanding the mechanisms. Cyclosporin A (CyA), a selective immunosuppressive drug used for organ transplantation, was selected as the drug in this study. CyA is a neutral lipophilic cyclic peptide composed of 11 amino acids and is slightly soluble in water.[22,23] In recent years, the developed pharmaceutical ingredients found in the screening study have become increasingly complex of chemical structure, large molecular weight, and hydrophobic for enhancing the pharmacological effects. Unfortunately, this results in poor water solubility. To overcome the poor solubility, a variety of the strategies to improve the solubility has been studied to develop formulations for oral, parenteral, and ocular administrations. Chen *et al*. recently discovered significant enhancement of CyA solubility to 702.5 $\mu g\ mL^{-1}$ using entrapment into 5wt%-P407, while that without P407 was determined to be 20.6 $\mu g\ mL^{-1}$ as extremely insoluble in water.[24]

Effects of drug entrapment into the nanocarrier on the interaction were explored by comparing the interaction potential surface between the P407 micelles with/without the drug. In addition, investigation based on density functional theory (DFT) calculation and dynamic light scattering (DLS) provided a deeper insight into the extremely stable dispersion of the nanocarrier on the basis of the contribution of the constituent monomers of the polymeric micelle.

RESULTS AND DISCUSSION

In aqueous solutions, the copolymer forms a spherical micelle above the critical micelle concentration (CMC). As represented by the schematic in Figure 1, hydrophobic and hydrophilic parts of the copolymer form the inner core and outer shell of the micelle, respectively. Figure 1 shows the SAXS profiles for P407 in H_2O. CMC of P407 at 25 °C was reported as 0.7,[25] 2.0,[10] and 2.5wt%,[10] depending on the determination methods. At 0.5 and 1.0wt%, a sharp increase in SAXS was observed below $q = 0.1$ nm^{-1}, where q is the scattering parameter defined by $4\pi\sin\theta/\lambda$ (2θ: scattering angle, λ: wavelength of X-rays). Bogomolova *et al*. have reported that the size splits into single molecules (*ca.* 3 nm in radius) and their aggregates (100–150 nm in radius) below critical micelle temperature (CMT).[8] The sharp increase in SAXS corresponds to the literature result, namely SAXS caused by micelle precursors of large polymer-chain aggregates. Above 2.0wt%, the SAXS having valley at $q = 0.45$ nm^{-1} indicates that micelles with the uniform structure were formed. With increasing concentrations, the depth of the valley at $q = 0.45$ nm^{-1} became deeper, indicating that the size uniformity became higher in the condensed region, as discussed by Kataoka *et al*.[1] The contribution of small-size Gaussian coil and blob in the micelle was mainly observed approximately above $q = 0.6$ nm^{-1}.[6,26]

Micelle–micelle distance in the dilute region is enlarged compared to the sum of the inner core and outer shell size, while the inter-micelle distance is equivalent to their diameter in the higher concentration.[27-29] With increasing concentrations, the peak in the SAXS around $q = 0.3$ nm^{-1} shifted to the higher q-region, which indicates shortening micelle–micelle distance. The concentration dependence of the SAXS corresponds to the previously proposed micelle–micelle structure represented by the schematic in Figure 1.

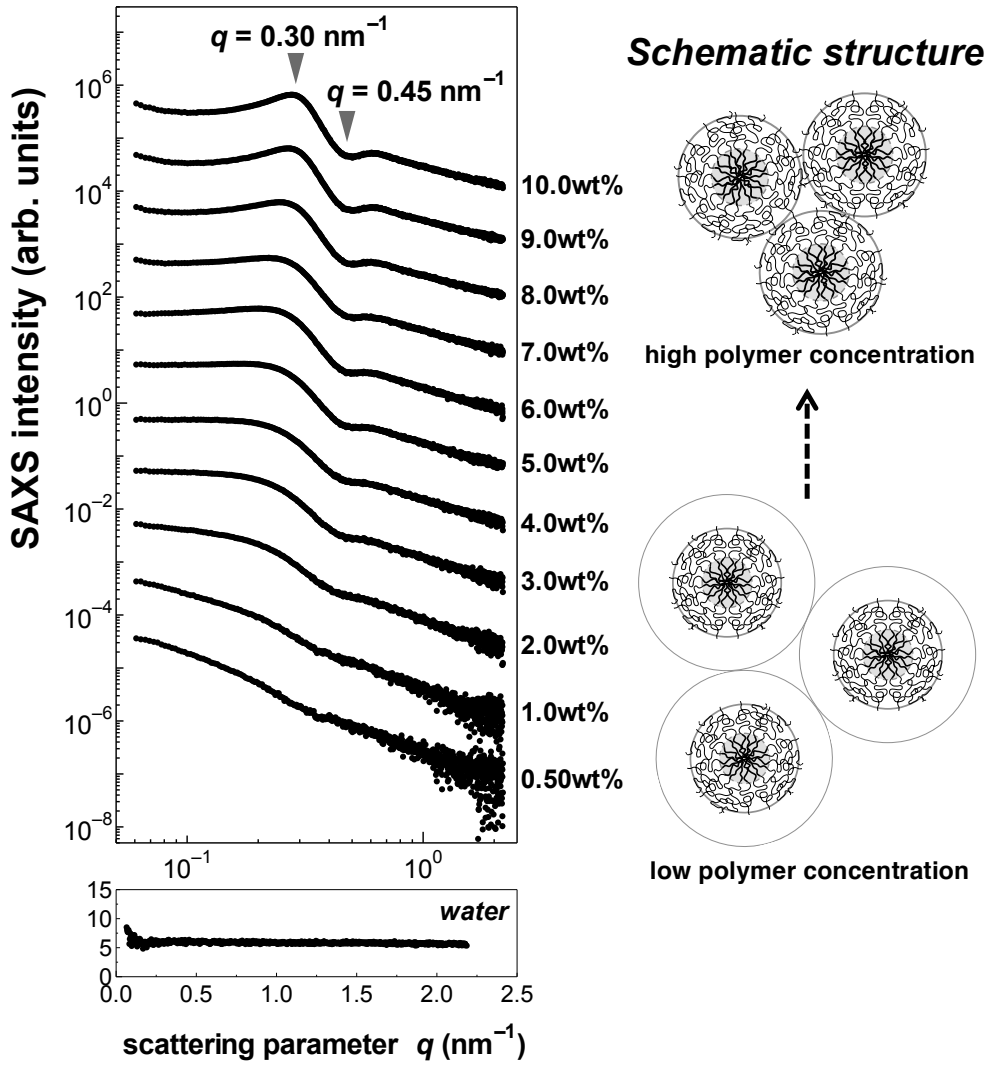

Figure 1 Concentration dependence of the SAXS profiles for neat P407 in H_2O at 25 °C and the SAXS for neat water providing the small-angle resolution. The right-hand side figure shows a conceptual representation of polymeric micelle and micelle–micelle structure.

Figure 2(a) shows the SAXS profiles under the presence of CyA (Figure 2(b)). As shown in Figure 2(c), the SAXS of the 10wt%-P407 system was reproduced by considering contributions of the micelle, small-size Gaussian coil, blob in the micelle, and micelle–micelle interference effect, according to the literature knowledge.[6,26,30] Contribution of micelle aggregates was additionally considered in the high concentration region. Micelle structure of P85 with $EO_{25}PO_{40}EO_{25}$ has been precisely investigated using the effective hard-sphere repulsive model.[31] The observed aggregation between the P407 micelles could be caused by the expanded outer shell composed of the long polymer chain, EO_{101}, of P407. Figure 2(d) shows the concentration dependence of the solved structure factor $S(q)$, which gives the spatial structure between the scatterers. $S(q)$ for neat P407 micelles calculated using the same procedure is shown in Figure S1. The evaluated $S(q)$s were used in input data of the present MPF theory.

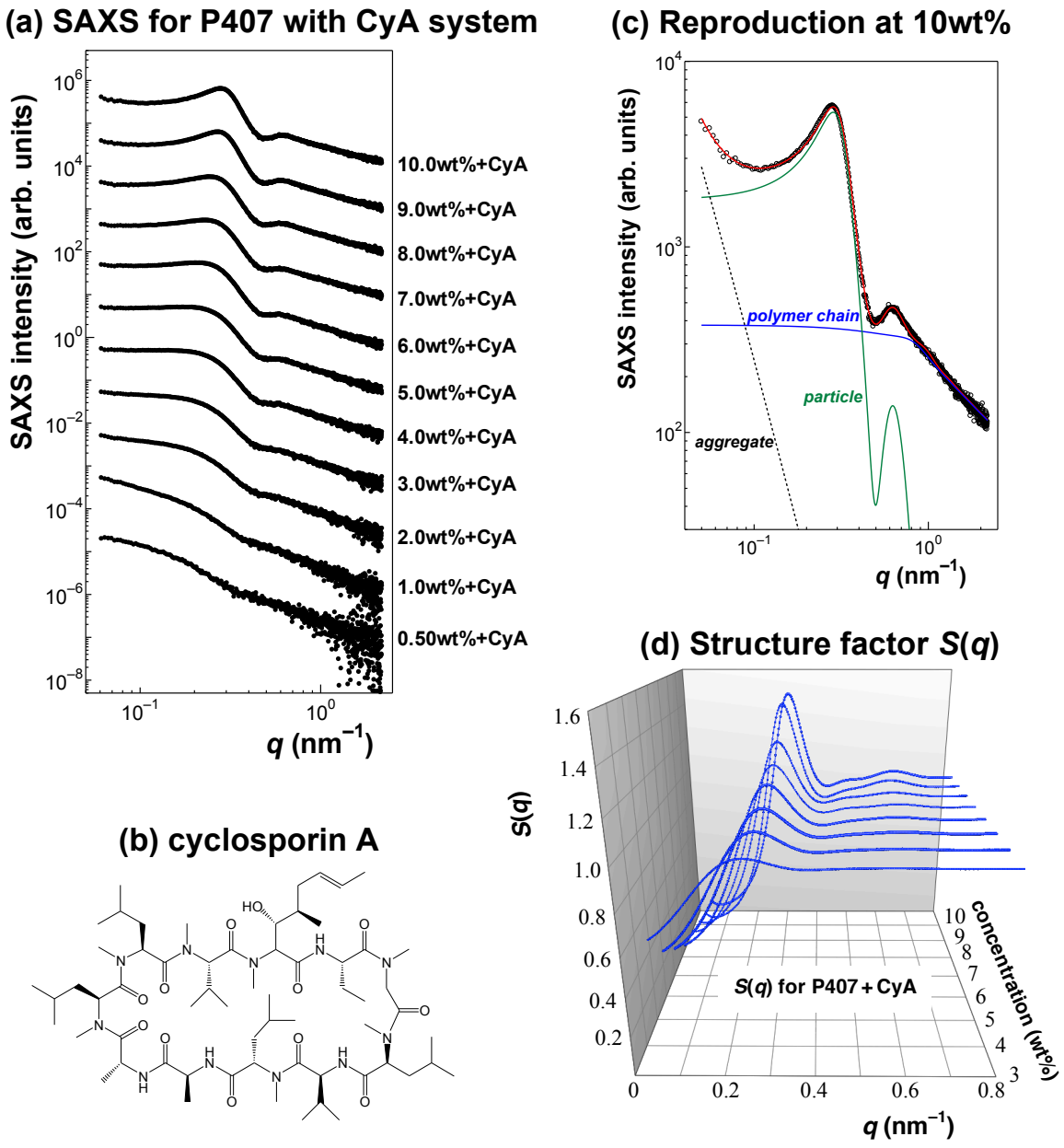

Figure 2 (a) Concentration dependence of the SAXS profiles for P407 with CyA in H_2O at 25 °C. (b) The chemical structure of CyA. (c) Reproduction of the SAXS profile of the 10wt%-P407 system. The open circles and solid red line represent the experimental SAXS data and the fitted total scattering, respectively. (d) Concentration dependence of the evaluated $S(q)$ for CyA-entrapped P407 micelles.

The interaction potential surface was determined by combining the experimental $S(q)$ and the MPF theory. Figures 3(a) and (b) show the results of the interaction potential surface between the micelles, $V(r)$, for neat P407 micelles and CyA-entrapped P407 micelles, respectively. The potential curves sharply arise at the contact region due to the overlap between the micelles. As shown in Figure 3, at 3wt%, the gradual decrease in repulsive force remained over 10 nm (~30 nm in intermicelle distance) far from the contact region between micelles. The repulsive force was also observed at 4 and 5wt% up to 27 nm in intermicelle distance. This long-range repulsion results in the extremely stable dispersion of the P407 micelles in the dilute region.

In contrast, shallow and wide minima were identified at high concentrations of 8, 9, and 10wt%. The depth of the minimum at 10.0wt% was estimated to be $V(r) \approx -0.5\ k_{\mathrm{B}}T$. The weak attractive force remained *ca.* 25 nm continuously ranging from 22 to 47 nm in intermicelle distance r (partially out of range of Figure 3). It was proposed that this long-range attractive interaction leads to the specific aggregation behavior of the micelles such as gelation and formation of high dimension structure in the condensed phase.[3]

The repulsive force in the potential curves was reduced around 20 nm in intermicelle distance in the dilute region, especially at 3wt%. In star-polymer like particles, namely polymer-chain-grafted nanoparticles, the repulsive force in the contact region is monotonously increased as the particles approach each other.[32,33] The reduction in repulsive force was specifically identified in the polymeric micelle. Moreover, also in high concentrations of 8, 9, and 10wt%, the repulsive force around 20 nm in intermicelle distance was quite lower than that for star-polymer like particles.[32,33] Liu *et al*. discussed the attractive force of micelle–micelle interaction in terms of surface adhesion and interpenetration by polymer chains of the outer layer to other micelles.[27] Bedrov *et al*. have reported the attractive interaction potential between the polymer chains of

PEO and PPO using theoretical calculation, showing stronger attraction between PEO chains than between PPO chains.[34] The investigations show the origin of attraction between polymeric micelles. The present study quantitatively revealed the *attractive* regime between the micelles in the vicinity of the contact region in solutions. The *attractive* regime means an interaction aspect not of a strong repulsive force but of a significantly weakened repulsion in a total potential curve caused by an attractive force contribution. This *attractive* regime was observed at high concentrations of 8, 9, and 10wt%, as well as the dilute region. It was suggested that the *attractive* regime and the long-range attractive force discussed above contribute to the high stability of the P407 hydrogel in the condensed phase used for the formulations and correspondingly to the sustained releasability of drugs.[3]

Effects of CyA entrapment on interaction potential surface between the micelles were identified by comparison between the micelles with and without the drug. At 3 and 4wt%, the repulsive force was reduced due to the incorporation. Conversely, in high concentration, the interaction between CyA-entrapped P407 micelles was analogous to that between neat P407 micelles. This is direct evidence that the drug-entrapped polymeric micelles remain in stable dispersion under the encapsulation of water-insoluble hydrophobic drugs in the inner core of the nanocarrier.

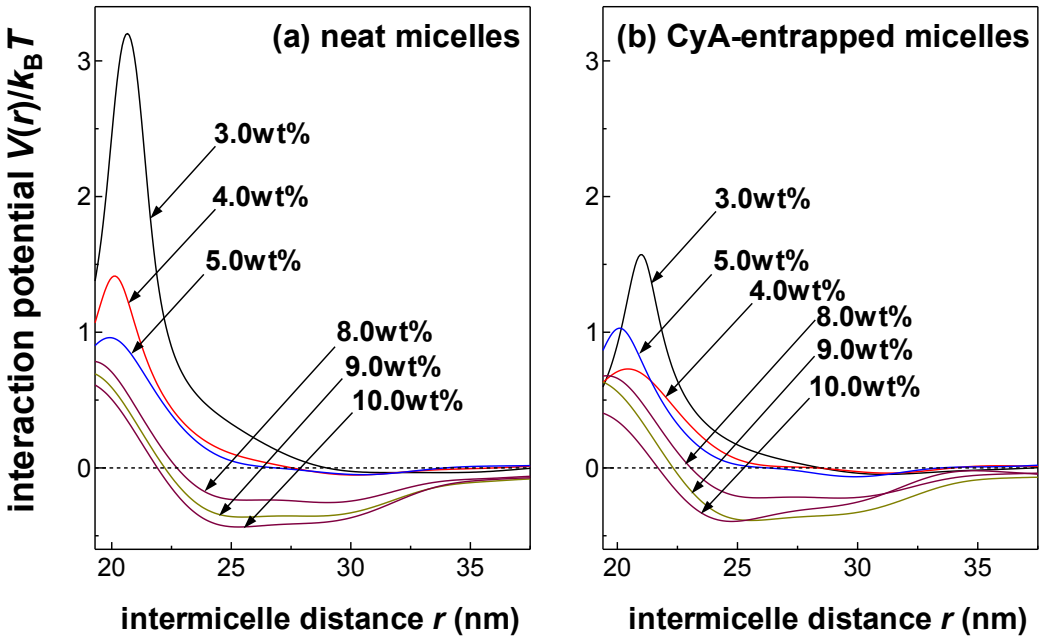

Figure 3 Change in the interaction potential curve, $V(r)/k_BT$, between (a) P407 micelles and (b) CyA-entrapped P407 micelles.

Figure 4(a) shows size distribution at typical P407 concentrations of 0.5, 7.0, and 10.0wt% obtained by the DLS analysis. The distribution is represented by the intensity-weighted frequency. The results at other concentrations and the size distribution of volume- or number-weighted frequency are shown in Figures S3–S8. In the dilute region of 0.5wt%, the distribution split into that with around ten nanometers and the large components, corresponding to the literature result[8] and the present SAXS data. The large size distribution was assigned as the micelle precursors of large polymer-chain aggregates, as discussed in Figure 1. The large size distribution with micrometers was also observed at 10.0wt% without filtering treatment, indicating the formation of aggregates composed of P407 micelles each other. The result supports the aggregation behavior observed in SAXS profiles and the attractive interaction in the high concentration region discussed in Figure 3. The distribution below 10 nm was assigned to be a component of P407 monomers. The frequency of monomer contribution was also observable at 7.0 and 10.0wt% even in the intensity-weighted distribution, indicating that the monomers sufficiently exist around the micelles. Figure 4(b) shows the concentration dependence of mean hydrodynamic diameter D_h for the monomers evaluated from the volume-weighted distribution shown in Figure S4. As shown in Figure 4(b), the monomer size was slightly decreased with increasing concentrations and remained constant at around 3.6 nm in the high concentration region. In the present condition, little change by the addition of CyA was observable in the monomer size.

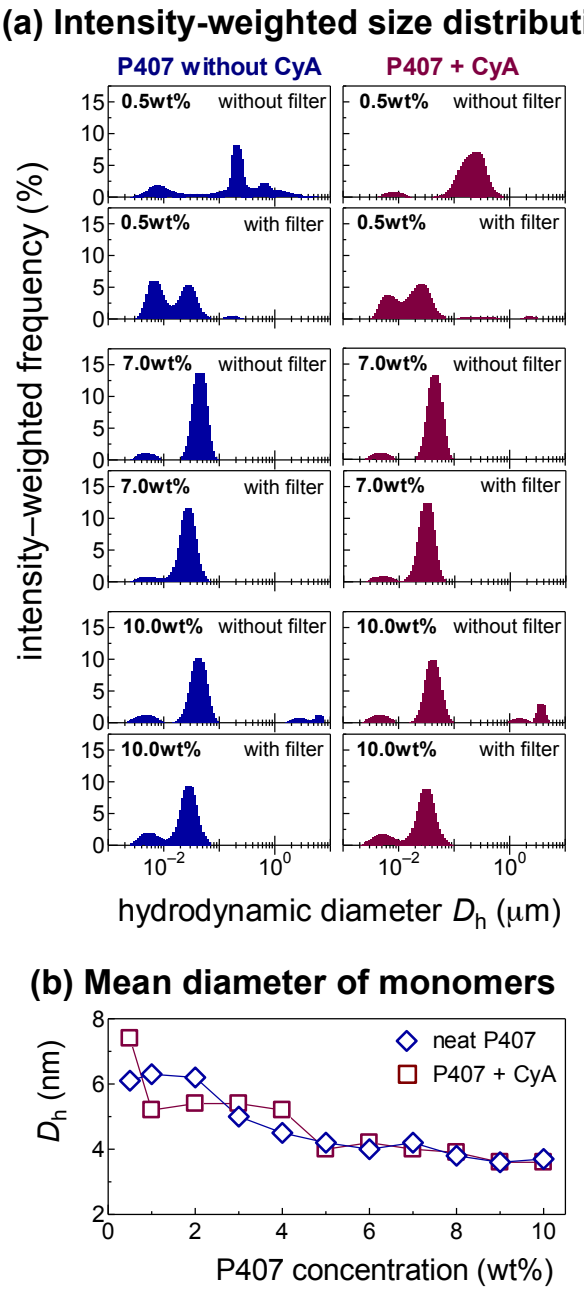

Figure 4 (a) Intensity-weighted size distribution as a function of the hydrodynamic diameter, D_h, obtained by the DLS analysis at 25 °C. Representation of "with filter" refers to 450 nm-filtering treatment applied to each sample immediately before the DLS measurements. (b) Concentration dependence of mean D_h of the monomers evaluated from the volume-weighted size frequency shown in Figure S4.

We considered that the extended inter-micelle distance and the repulsion in the dilute region represented by the schematic of Figure 1 are not explained only by the slight concentration dependence of the monomer size. To reveal a deeper insight into the origin of the repulsive force, we examined the effects of the monomers remaining in the solution on the interaction potential between the micelles using a coarse-grained model of polymer-colloid mixture. Figure 5(a) shows the results of DFT calculation for interaction potential curve, $V(r)$, and radial distribution function, $g_{cc}(r)$, between the modeled colloid particles. The DFT calculation was modeled with/without monomers, which identifies monomer contribution to the micelle–micelle structure. The parameters used in the DFT calculation are listed in Tables S2 and S3. As shown in Figure 5(a), the repulsive force in $V(r)$ was clearly reproduced by the monomer-presence model. On the other hand, $V(r)$ without monomers, which corresponds to the direct interaction between the model colloids, was inconsistent with the interactions discussed in Figure 3. As shown in Figure 5(a), the height around 20 nm in $g_{cc}(r)$ was lower than that without monomers due to the repulsive force. The DFT investigation demonstrated the intermicelle structure and the repulsion as follows: (1) essential monomer chain contribution to the extended separation between micelles in the dilute region, (2) requirement of attraction of monomers to micelle surface, rather than depletion effect,[35] and (3) contacted structure between the micelles in the condensed region even under the presence of enough monomer chains around micelles. The depletion force between colloidal particles has been well known as a typical effect of crowding agents on colloids. The necessary condition for the depletion force is that the crowding agents do not prefer the colloidal particles so that the crowders are excluded from the area between the colloidal particles. In contrast, if the crowding agents prefer the colloidal particle, a repulsive force between the colloidal particles is mediated by the preferential binding of crowders to the colloids.

Kulshreshtha *et al*. have investigated particle-particle interactions with a variation of athermal, weakly attractive, and strongly attractive interactions between grafted polymer to particle and matrix polymer in solution.[36] The result indicated that the repulsive force between the particles sharply arises with an increase in attraction between the grafted polymer and the matrix polymer. The repulsion aspect evaluated by the present DFT calculation corresponds to the graft-matrix model calculation.

The effects of monomer chains on interaction between colloid particles have been discussed on the basis of conceptual phenomena of monomer chains such as protective agent behavior,[37] protrusion,[38] and monomer chain exchange between micelles.[2,39] The result of the present DFT calculation is consistent with the literature knowledge. In the present model, effective contributions of these phenomena were taken into consideration *via* the monomer chains weakly bound to the modeled particles. Figure 5(b) represents the developed schematic of the micelle–micelle structure in the dilute region (3wt%), which was proposed by the determined $V(r)$ shown in Figure 3, the monomer structure by the DLS analysis shown in Figure 4, and the monomer contribution demonstrated by the DFT investigation.

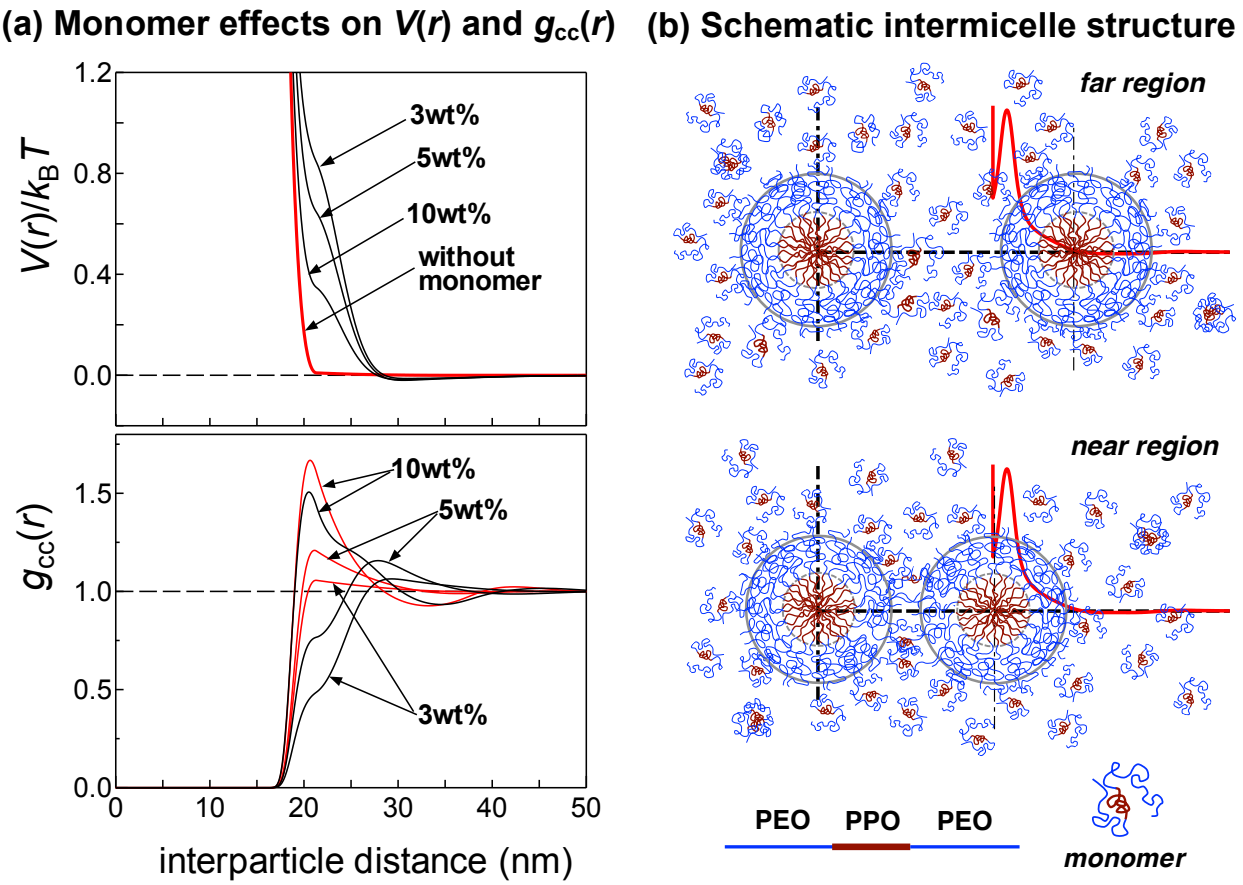

Figure 5 DFT investigation and the proposed schematic of micelle–micelle structure. (a) Interaction potential surface, $V(r)$, and radial distribution function, $g_{cc}(r)$, between the modeled particles. The black and red solid lines represent the results with and without monomers, respectively. In the $V(r)$ plot, the red line corresponds to $V(r)$ without monomers at 3, 5, and 10wt%. (b) Schematic representation of the micelle–micelle structure in the dilute region (3wt%), where the red solid curves represent the interaction potential surface between the P407 micelles at 3.0wt% discussed in Figure 3(a).

CONCLUSIONS

The interaction potential surface between drug-entrapped polymeric micelles was quantitatively determined by combining the SAXS method and the MPF theory without eliminating any interaction forces. The water-insoluble hydrophobic drug, CyA, was incorporated in P407 polymeric micelles. The long-range attractive force in the potential curves was revealed in the high concentration region. Moreover, the reduction in the repulsive force was identified in the vicinity of the contact region between the P407 micelles. The *attractive* regime unveiled in this study directly clarified the high stability of the hydrogel in the condensed phase used for the drug formulations and the important characteristics of the sustained releasability of drugs.

In the dilute region, the long-range repulsion in the potential curves was evaluated, which is related to the extremely stable dispersion of P407 micelles. DFT studies aimed at elucidating the long-range repulsion and the specific extended separation between the micelles demonstrated the significant contribution of the monomer chains and the attraction of monomers to the micelle surface. The developed schematic of micelle–micelle structure was proposed on the basis of the findings by the SAXS, the DLS, and the DFT calculation.

The present investigation directly clarified the high drug carrier efficiency in terms of interaction between the micelles. Given the findings of this study, we expect that the present approach will be applied to various types of drug-incorporated nanocarriers, and contribute to reveal the core mechanisms of the high drug carrier efficiency and develop nanocarriers with superior functions in drug delivery. The pharmaceutical property of drug-incorporated P407 formulation before and after administration should be discussed in more detail by evaluating the interaction potential surface at different conditions including temperature, pH, and salt concentration.

METHODS

SAXS measurements. The SAXS was measured using synchrotron radiation at the BL-6A station of the Photon Factory (PF) at the High Energy Accelerator Research Organization (KEK), Tsukuba.[40] The observable q-region of the SAXS was 0.06–2.2 nm^{-1}. The wavelength of the X-rays and the exposure time were set at 0.15 nm and 240 s, respectively. The X-ray absorption factors of the samples were measured simultaneously during the SAXS measurements using an in situ beam monitoring apparatus with a silicon photodiode device.[40,41]

DLS measurements. The DLS was acquired using a Microtrac UPA particle analyzer (Nikkiso Co., Japan; measurement range: 0.0008–6.5 μm) under the following conditions: measurement time, 180 s; repeat count, 3 times; temperature, 25 ºC. The hydrodynamic diameter was calculated using the Stokes–Einstein relation.[42] The viscosity of H_2O at 25 °C was used for the viscosity correction in the size evaluation.

MPF theory. In this method, instead of introducing specific model-potential functions, we applied the random phase approximation, as an additional closure to the Ornstein–Zernike integral equation. Moreover, we introduced a reference term for the hard-sphere (HS) with a diameter d_{HS} based on the size of the micelles, which was experimentally determined from the obtained SAXS profile. More details on the MPF theory are provided in the SI.

Coarse-grained modeling for the DFT calculation. We modeled the polymeric micelle solution as a system of the nanoparticles immersed in a polymer solution with an implicit solvent. By varying the number density of the polymer chain such that the concentration dependence of $S(q)$

can be reproduced without changing the interaction potentials of the system, we applied a DFT to that system[43,44] to calculate the $V(r)$ and pair distribution functions. In these DFT calculations, we employed the number density of the polymeric micelle determined for each concentration by the MPF calculation was used. The details of the model and the DFT calculation are provided in the SI.

ASSOCIATED CONTENT

Supporting Information

The Supporting Information is available free of charge at https://pubs.acs.org.

Experimental details for the material, preparation of the solutions, the SAXS, and the DLS; procedures of the MPF calculation and the DFT calculation; appendix for the present DFT calculation.

AUTHOR INFORMATION

Corresponding Authors

*Email: T Morita (moritat@faculty.chiba-u.jp), or K Higashi (ken-h@faculty.chiba-u.jp, or T Sumi (sumi@okayama-u.ac.jp)

Author Contributions

T.M., K.H., and K.M. conceived the project. S.M. and Z.C. prepared the sample solutions. S.M. and K.H. performed the DLS measurement. T.M. carried out the SAXS experiment. The DFT calculation was done by T.S. The interaction potential surface was evaluated by T.S., T.M., and

H.I. H.I. investigated the related literature. The manuscript was written by T.M. with contributions from all authors. All authors commented on the manuscript.

Funding Sources

JSPS grant-in-aid for Scientific Research (KAKENHI)

Notes

The authors declare no competing financial interest.

ACKNOWLEDGEMENTS

We are grateful to PF at KEK for providing the opportunity to perform the SAXS experiments (Proposal No. 2019G672). We appreciate Dr. Kenkichi Sasaki and Mr. Yoshiaki Yamazaki (Entegris Co., Ltd.) for their special support in acquiring DLS using homodyne optics and a high sensitive detector. This work was partially supported by a JSPS grant-in-aid for Scientific Research (KAKENHI).

ABBREVIATIONS

CMC, Critical micelle concentration; CMT, Critical micelle temperature; DFT, Density functional theory; DLS, Dynamic light scattering; HS, Hard-sphere; MPF, Model-potential-free; SAXS, Small-angle X-ray scattering

REFERENCES

(1) Kataoka, K.; Harada, A.; Nagasaki, Y. Block Copolymer Micelles for Drug Delivery: Design, Characterization and Biological Significance. *Adv. Drug Deliv. Rev.* **2001**, *47*, 113.

(2) Owen, A. C.; Chan, D. P. Y.; Shoichet, M. S. Polymeric Micelle Stability. *Nano Today* **2012**, *7*, 53.

(3) Dumortier, G.; Grossiord, J. L.; Agnely, F.; Chaumeil, J. C. A Review of Poloxamer 407 Pharmaceutical and Pharmacological Characteristics. *Pharm. Res.* **2006**, *23*, 2709.

(4) Sanada, Y.; Akiba, I.; Sakurai, K.; Shiraishi, K.; Yokoyama, M.; Mylonas, E.; Ohta, N.; Yagi, N.; Shinohara, Y.; Amemiya, Y. Hydrophobic Molecules Infiltrating into the Poly(ethylene glycol) Domain of the Core/Shell Interface of a Polymeric Micelle: Evidence Obtained with Anomalous Small-Angle X-ray Scattering. *J. Am. Chem. Soc.* **2013**, *135*, 2574.

(5) Bayati, S.; Galantini, L.; Knudsen, K. D.; Schillén, K. Complexes of PEO-PPO-PEO Triblock Copolymer P123 and Bile Salt Sodium Glycodeoxycholate in Aqueous Solution: A Small Angle X-ray and Neutron Scattering Investigation. *Colloids Surf. A: Physicochem. Eng. Asp.* **2016**, *504*, 426.

(6) Valero, M.; Castiglione, F.; Mele, A.; da Silva, M. A.; Grillo, I.; Gonzalez-Gaitano, G.; Dreiss, C. A. Competitive and Synergistic Interactions between Polymer Micelles, Drugs, and Cyclodextrins: The Importance of Drug Solubilization Locus. *Langmuir* **2016**, *32*, 13174.

(7) Feitosa, V. A.; Almeida, V. C.; Malheiros, B.; Castro, R. D.; Barbosa, L. R. S.; Cerize, N. N. P.; Rangel-Yagui, C. Polymeric Micelles of Pluronic F127 Reduce Hemolytic Potential of Amphiphilic Drugs. *Colloids Surf. B: Biointerfaces* **2019***, 180*, 177.

(8) Bogomolova, A.; Hruby, M.; Panek, J.; Rabyk, M.; Turner, S.; Bals, S.; Steinhart, M.; Zhigunov, A.; Sedlacek, O.; Stepanek, P.; Filippov, S. K. Small-Angle X-ray Scattering and Light Scattering Study of Hybrid Nanoparticles Composed of Thermoresponsive Triblock Copolymer F127 and Thermoresponsive Statistical Polyoxazolines with Hydrophobic Moieties. *J. Appl. Cryst*. **2013**, *46*, 1690.

(9) Singla, P.; Singh, O.; Sharma, S.; Betlem, K.; Aswal, V. K.; Peeters, M.; Mahajan, R. K. Temperature-Dependent Solubilization of the Hydrophobic Antiepileptic Drug Lamotrigine in Different Pluronic Micelles a Spectroscopic, Heat Transfer Method, Small-Angle Neutron Scattering, Dynamic Light Scattering, and in Vitro Release Study, *ACS Omega* **2019**, *4*, 11251.

(10) Desai, P. R.; Jain, N. J.; Sharma, R. K.; Bahadur, P. Effect of Additives on the Micellization of PEO/PPO/PEO Block Copolymer F127 in Aqueous Solution. *Colloids Surf. A*: *Physicochem*. *Eng*. *Asp.* **2001**, *178*, 57.

(11) Basak, R.; Bandyopadhyay, R. Encapsulation of Hydrophobic Drugs in Pluronic F127 Micelles: Effects of Drug Hydrophobicity, Solution Temperature, and pH. *Langmuir* **2013**, *29*, 4350.

(12) Hamley, I. W.; Castelletto, V. Small-Angle Scattering of Block Copolymers: in the Melt, Solution and Crystal State. *Prog. Polym. Sci.* **2004**, *29*, 909.

(13) Sumi, T.; Imamura, H.; Morita, T.; Nishikawa, K. A Model-Free Method for Extracting Interaction Potential between Protein Molecules Using Small-Angle X-Ray Scattering. *J. Mol. Liq*. **2014**, *200*, 42.

(14) Sumi, T.; Imamura, H.; Morita, T.; Isogai, Y.; Nishikawa, K. Model-Potential-Free Analysis of Small Angle Scattering of Proteins in Solution: Insights into Solvent Effects on Protein–Protein Interaction. *Phys. Chem. Chem. Phys.* **2014**, *16*, 25492.

(15) Morita, T.; Uehara, N.; Kuwahata, K.; Imamura, H.; Shimada, T.; Ookubo, K.; Fujita, M.; Sumi, T. Interaction Potential between Biological Sensing Nanoparticles Determined by Combining Small-Angle X-ray Scattering and Model-Potential-Free Liquid Theory. *J. Phys. Chem. C.* **2016**, *120*, 25564.

(16) Morita, T.; Ogawa, Y.; Imamura, H.; Ookubo, K.; Uehara, N.; Sumi, T. Interaction Potential Surface between Raman Scattering Enhancing Nanoparticles Conjugated with a Functional Copolymer. *Phys. Chem. Chem. Phys.* **2019**, *21*, 16889.

(17) Amano, K.-I.; Sawazumi, R.; Imamura, H.; Sumi, T.; Hashimoto, K.; Fukami, K.; Kitaoka, H.; Nishi, N.; Tetsuo Sakka, T. An Improved Model-Potential-Free Analysis of the Structure Factor Obtained from a Small-Angle Scattering: Acquisitions of the Pair Distribution Function and the Pair Potential. *Chem. Lett*. **2020**, *49*, 1017.

(18) Derjaguin, B.; Landau, L. Theory of the Stability of Strongly Charged Lyophobic Sols and of the Adhesion of Strongly Charged-Particles in Solutions of Electrolytes. *Prog. Surf. Sci.* **1993**, *43*, 30.

(19) Verwey, E. J. W.; Overbeek, J. T. G. *Theory of the Stability of Lyophobic Colloids*; Elsevier, Amsterdam, 1948.

(20) Julius, K.; Weine, J.; Gao, M.; Latarius, J.; Elbers, M.; Paulus, M.; Tolan, M.; Winter, R. Impact of Macromolecular Crowding and Compression on Protein–Protein Interactions and Liquid–Liquid Phase Separation Phenomena. *Macromolecules* **2019**, *52*, 1772.

(21) Liu, Y.; Fratini, E.; Baglioni, P.; Chen, W.-R.; Chen, S.-H. Effective Long-Range Attraction between Protein Molecules in Solutions Studied by Small Angle Neutron Scattering. *Phys. Rev. Lett.* **2005**, *95*, 118102.

(22) Survase, S.A.; Kagliwal, L.D.; Annapure, U.S.; Singhal R.S. Cyclosporin A - A review on Fermentative Production, Downstream Processing and Pharmacological Applications. *Biotechnology Advances*, **2011**, *29*, 418.

(23) Fatouros, D.G.; Karpf, D.M.; Nielsen, F.S.; Mullertz, A. Clinical Studies with Oral Lipid Based Formulations of Poorly Soluble Compounds. *Ther Clin Risk Manag.* **2007**, *3*, 591.

(24) Chen, Z.; Ueda, K.; Higashi, K.; Moribe, K. Molecular-Level Evaluation of the Transition from Amorphous to Crystalline Nanoparticles in Cyclosporin A Nanosuspension Prepared by Wet Bead Milling with Poloxamer 407 (in preparation of manuscript).

(25) Alexandridis, P.; Holzwarth, J. F.; Hatton, T. A. Micellization of Poly(ethylene oxide)-Poly(propylene oxide)-Poly(ethylene oxide) Triblock Copolymers in Aqueous Solutions: Thermodynamics of Copolymer Association. *Macromolecules* **1994**, *27*(9), 2414.

(26) Matsuoka, H.; Yamamoto, Y.; Nakano, M.; Endo, H.; Yamaoka, H.; Zorn, R.; Monkenbusch, M.; Richter, D.; Seto, H.; Kawabata, Y.;Nagao, M. Neutron Spin-Echo Study of the Dynamic Behavior of Amphiphilic Diblock Copolymer Micelles in Aqueous Solution. *Langmuir* **2000**, *16*, 9177.

(27) Liu, Y. C.; Chen, S. H.; Huang, J. S. Small-Angle Neutron Scattering Analysis of the Structure and Interaction of Triblock Copolymer Micelles in Aqueous Solution. *Macromolecules* **1998**, *31*, 2236.

(28) Yang, L.; Alexandridis, P.; Steytler, D. C.; Kositza, M. J.; Holzwarth, J. F. Small-Angle Neutron Scattering Investigation of the Temperature-Dependent Aggregation Behavior of the Block Copolymer Pluronic L64 in Aqueous Solution. *Langmuir* **2000**, *16*, 8555.

(29) Liang Guo, L.; Colby, R. H.; Lin, M. Y.; Gregory P. Dado, G. P. Micellar Structure Changes in Aqueous Mixtures of Nonionic Surfactants. *J. Rheol.* **2001**, *45*, 1223.

(30) Glatter, O.; Kratky, O. *Small Angle X-Ray Scattering*; Academic Press, New York, 1982.

(31) Pedersen, J. S.; Gerstenberg, M. C. The Structure of P85 Pluronic Block Copolymer Micelles Determined by Small-Angle Neutron Scattering. *Colloids Surf. A: Physicochem. Eng. Asp.* **2003**, *213*, 175.

(32) Likos, C. N.; Löwen, H.; Watzlawek, M.; Abbas, B.; Jucknischke, O.; Allgaier, J.; Richter, D. Star Polymers Viewed as Ultrasoft Colloidal Particles, *Phys. Rev. Lett.* **1998**, *80*, 4450.

(33) Vlassopoulos, D.; Cloitre, M. Tunable Rheology of Dense Soft Deformable Colloids. *Curr. Opin. Colloid Interface Sci.* **2014**, *19*, 561.

(34) Bedrov, D.; Ayyagari, C.; Smith, G. D. Multiscale Modeling of Poly(Ethylene Oxide)–Poly(Propylene Oxide)–Poly(Ethylene Oxide) Triblock Copolymer Micelles in Aqueous Solution. *J. Chem. Theory Comput.* **2006**, *2*, 598.

(35) Asakura, S.; Oosawa, F. On Interaction between Two Bodies Immersed in a Solution of Macromolecules. *J. Chem. Phys.* **1954**, *22*, 1255.

(36) Kulshreshtha, A.; Jayaraman, A. Dispersion and Aggregation of Polymer Grafted Particles in Polymer Nanocomposites Driven by the Hardness and Size of the Grafted Layer Tuned by Attractive Graft–Matrix Interactions. *Macromolecules* **2020**, *53*, 1302.

(37) Gregory J. *Effects of Polymers on Colloid Stability.* In The Scientific Basis of Flocculation. NATO Advanced Study Institutes Series (Series E: Applied Science) vol 27; : Ives K. J., Ed.; Springer: Dordrecht, 1978; pp 101-130.

(38) Israelachvili, J. N. *Intermolecular and Surface Forces*; Academic Press, London, 1991.

(39) Turq, P.; Drifford, M.; Hayoun, M.; Perera, A.; Tabony, J. Influence of Monomer-micelle Exchange on Micelle Diffusion. *J. Phys. (Paris), Lett.* **1983**, *44*, 471.

(40) Takagi, H.; Igarashi, N.; Mori, T.; Saijo, S.; Ohta, H.; Nagatani, Y.; Kosuge, T.; Shimizu, N. Upgrade of Small Angle X-ray Scattering Beamline, BL-6A at the Photon Factory. *AIP Conf. Proc.* **2016**, *1741*, 030018, DOI: 10.1063/1.4952841

(41) Morita, T.; Tanaka, Y.; Ito, K.; Takahashi, Y.; Nishikawa, K. Apparatus for the Simultaneous Measurement of the X-Ray Absorption Factor Developed for a Small-Angle X-Ray Scattering Beamline. *J. Appl. Cryst.* **2007**, *40*, 791.

(42) Einstein, A. *Investigations on the Theory of the Brownian Movement*; Dover Publications Inc., New York, 1956.

(43) Sumi, T.; Hirata, F. A Density-Functional Theory for Polymer Liquids Based on the Interaction Site Model. *J. Chem. Phys.* **2003**, *118*, 2431.

(44) Sumi, T.; Sekino, H. A Cooperative Phenomenon between Polymer Chain and Supercritical Solvent: Remarkable Expansions of Solvophobic and Solvophilic Polymers. *J. Chem. Phys.* **2005**, *122*, 194910.

For Table of Contents Only